CHAPTER 2

ANALYSIS OF SIDE COUPLED CAVITY (SCC) STRUCTURE*

*Part of this work was published as:

Prabhakar Tripathi, A. Kumar, S. Dwivedi, and Pradip Kumar Jain, "Equivalent Circuit Analysis of the Side-Coupled Cavity Structure," *IEEE Transactions on Plasma Science, vol. 48, no. 10, pp. 3501-3509, Oct. 2020, DOI:10.1109/TPS.2020.3022281*

CHAPTER 2

ANALYSIS OF SIDE COUPLED CAVITY (SCC) STRUCTURE

2.1. Overview

In this chapter, the resonating frequency associated with the side coupled-cavity (SCC) is theoretically explored with the help of an equivalent circuit approach. This study is focused to estimate the coefficient of magnetic coupling factor in the context of its structural parameters, which has so far been experimentally evaluated. An empirical formula is proposed to calculate the fundamental-mode frequency that includes the effect of the magnetic-coupling factor, which has not been considered in the previously reported researches. To perform this research study, the SCC is designed and simulated with the help of the "CST Studio Suite". The results obtained from the proposed empirical formula are compared with the simulation result to verify the theoretical analysis. The relative error is less than 1%, which indicates that there is a good agreement between the results and validates the performed analysis.

2.2. Introduction

The SCC is used as a slow-wave RF interaction structure in HPM devices and is mainly used in linear accelerators and reltron oscillators [Knapp *et al.* (1965), Knapp (1976), Amaldi (1999), Miller (2006), Benford *et al.* (2007), Hamm *et al.* (2012)]. It is imperative to perform an accurate and in-depth study of its key component, i.e. RF interaction structure. The dispersion relation is an excellent tool that provides information about the EM and RF behavior of the RF interaction cavity and highlights the structural dependencies that help in the design and development of the system.

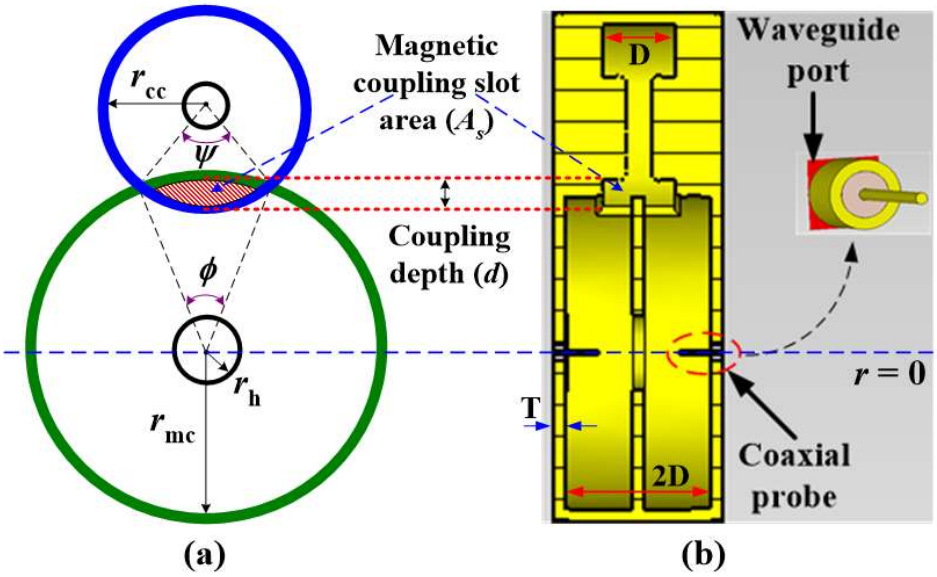

Figure 2.1: Different cross-sectional view of SCC: (a) lateral cross-section view, and (b) longitudinal cross-section view with a coaxial probe.

Fig. 2.1 shows the different cross-sections of the unit cell of the SCC structure i.e. Fig. 2.1 (a) shows the lateral cross-section, while Fig. 2.1 (b) shows the longitudinal cross-section. The geometry of the unit cell of the SCC structure consists of one coupled cavity, one main pillbox cavity, and three metal discs. A metal disc placed in the middle of the main pillbox box cavity separates the main pillbox box cavity into two identical cavities known as the front and back main pillbox cavity. In SCC, the coupled-cavity mounted at the periphery of the main pillbox cavity is used to provide a magnetic coupling between the adjacent main cavities, while the electric coupling is present due to a hole present for beam passage at the center of the metal disc.

This multi-cavity resonating system resonates at three modes i.e. 0-mode, π/2-mode, and π-mode. The desired mode for operation in all these three modes is π/2-mode since it is the only unstable mode [Miller *et al.* (1992), Knapp *et al.* (1968)]. The major

advantage associated with SCC is that it has lower sensitivity to frequency deviation and cell-to-cell phase deviation with higher dimensional tolerance [Nepal *et al.* (1991)].

The SCC finds its application as an RF interaction structure in the reltron oscillator. Reltron is a slow-wave microwave oscillator, which generates high-power electromagnetic radiation from a few hundreds of megawatt range with a pulse duration of a few microseconds, and a pulse repetition rate (PRR) of <100 Hz. The reltron is simple, compact in size, lightweight, long life, high PRR, and highly efficient device [Miller *et. al.* (1995)]. The fundamental resonating mode frequency (i.e. the frequency associated with the $\pi/2$-mode) of this complex multi-cavity slow-wave structure (SWS) mainly depends on the radius of the main pillbox cavity and the coefficient of magnetic coupling factor that exists between the adjacent main pillbox cavities.

There are various techniques, such as EM simulation software, dispersion relations, and equivalent circuit approaches, which are typically used to estimate the EM behavior of the resonating structure. One approach can be through EM simulation, using commercial tools, such as “MAGIC,” “CST Studio Suite,” “HFSS,” and others. EM simulation tools are extensively used to visualize and analyze the electric field distributions associated with the different modes within the resonating structure. The dispersion relation is another approach generally used to calculate the resonating frequency of the resonating structure. In this approach, Maxwell’s equations are solved using appropriate boundary conditions to obtain the dispersion relation. However, this technique typically leads to a transcendental equation, which is solved numerically. The third approach can be the equivalent circuit analytical approach to calculate the resonating frequency associated with different resonating modes of the resonating structure.

Knapp *et al.* reported an analytical method to calculate the resonating frequency of SCC; however, in this analysis, the effect of the coupling depth on the resonating frequency was not considered [Knapp *et al.* (1965)]. Roy *et al.* considered the effect of the magnetic coupling depth and calculated the coefficient of the magnetic coupling factor (k) with the help of the magnetic field present at the center of the slot of the coupling cavity; however, it did not include any structural parameter [Roy *et al.* (1993)]. Soh *et al.* also performed an equivalent circuit analysis to investigate the resonant frequency of the SCC but they did not consider the effect of magnetic coupling depth in their analysis [Soh *et al.* (2010)]. Laneve *et al.* developed the computer code for designing the side-coupled cavities of a linear accelerator. This developed computer code is based on the finite element method (FEM) and multi-objective particle swarm optimization approach that automatically optimizes the geometry of the accelerating tank [Laneve *et al.* (2018)]. For calculating the coefficient of the magnetic coupling factor present in the SCC, no theoretical work has yet been reported and its calculation relies only on experimental measurements.

To fill this research gap, in this chapter we have developed an expression to calculate the coefficient of magnetic coupling factor (k) in terms of structural parameters of SCC considering magnetic coupling depth. Also, an empirical expression is proposed to calculate the fundamental resonance mode frequency of SCC considering the effect of magnetic coupling depth. To validate the proposed analysis, the computational values obtained from the developed expressions have been compared to the results obtained from EM simulations.

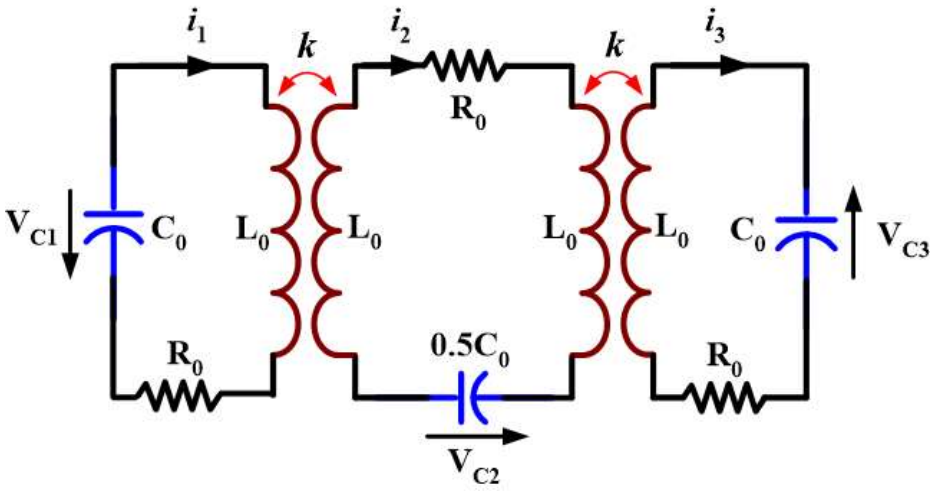

Figure 2.2: Equivalent circuit model of the SCC.

2.3. Equivalent Circuit Analysis

The geometry of SCC is comprised of one main pillbox cavity, and three metal discs, and one coupled-cavity [Knapp *et al.* (1965)]. The main pillbox cavity is divided into two identical adjacent main pillbox cavities named as front and back main pillbox cavity by inserting a metal disc at the front end, rear end, and at the center of the main cavity. These adjacent main pillbox cavities are magnetically (or inductively) coupled through the radially connected coupled-cavity [Knapp *et al.* (1965), Miller *et al.* (1992)]. The equivalent circuit model for the SCC is shown in Fig. 2.2, which consists of three RLC-circuits [Knapp *et al.* (1968), Soh *et al.* (2010)]. The middle RLC-circuit represents the coupled cavity while the leftmost and rightmost RLC-circuits represent the front and back main pillbox cavities of the SCC, respectively. In the equivalent circuit model, the currents in the inductor and voltage across the capacitor represent the magnetic field and electric field present in the respective cavities. The same circuit model is also used for $(N+1)$ inductively coupled linear accelerators structure [Miller (2006)]. In $(N+1)$ inductively

coupled cavity structure (N) represents the number of the main pillbox cavity, which is going to be coupled (always an even number), and $(+1)$ represents the coupled-cavity used for providing the magnetic coupling between them. Since the radius of the main pillbox cavity is nearly 1.5 times the coupled cavity and the capacitance is directly proportional to the square of the radius, therefore, the capacitance of the main pillbox cavity (C_0) is selected to be twice the capacitance of the coupled cavity ($0.5 \times C_0$) [Miller (2006), Soh *et al.* (2010)]. The capacitance associated with coupled-cavity and main pillbox cavity has been described in the design methodology section of Chapter-4. Also, the inductance of the coupled cavity is generated due to the trapped magnetic field (i.e. from both adjacent main pillbox cavities), therefore the coupled cavity is assigned the same inductance (L_0) for the front and back main pillbox cavities. The magnetic field induces a surface current to flow along the cavity walls and the cavity wall has finite conductivity, therefore a resistance (R_0) has been introduced which represents the losses of the cavity.

To know the electric field distribution within the SCC, the SCC structure is modeled in "CST Studio Suite" according to the structural dimension mentioned in Table 2.1. The designed structure is then simulated using CST's eigenmode solver module and its result is shown in Fig. 2.3. From the figure, it can be seen that for 0-mode the electric field in the coupled cavity and the main pillbox cavity are in the same phase while for the π-mode the electric field present in the coupled cavity and the main pillbox cavity are 180° out of phase. For the π/2-mode, the electric field present in the coupled cavity is nearly zero, and the electric fields present in the adjacent main pillbox cavities have a phase difference of 180°. In the SCC, infinite numbers of discrete modes are excited and every discrete mode has its unique resonating frequency.

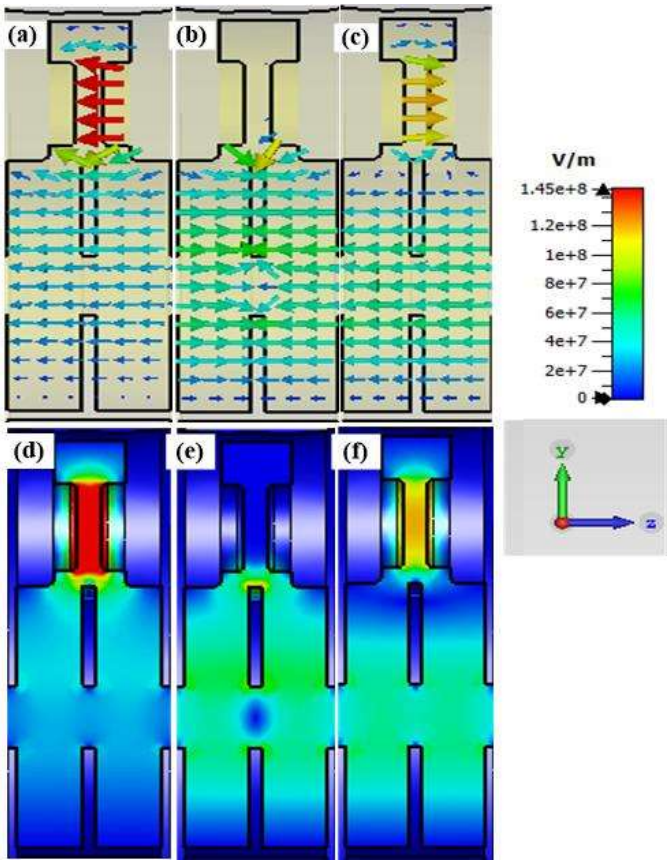

Figure 2.3: Electric field distribution in the SCC: (a), (b), and (c) shows the vector plot of with 0, π/2, and π-mode respectively while (d), (e), and (f) shows the contour plot of the 0, π/2, and π-mode respectively.

Table 2.1: Structural specification of the SCC.

Structural specification	
Main cavity radius (r_{mc})	38.85 mm
Coupled cavity radius (r_{cc})	25.51 mm
Length of main pillbox cavity $(2\times D)$	36.00 mm
Length of coupled-cavity (D)	18.00 mm
Disc hole radius (r_h)	12.60 mm
Thickness of disc (T)	03.00 mm

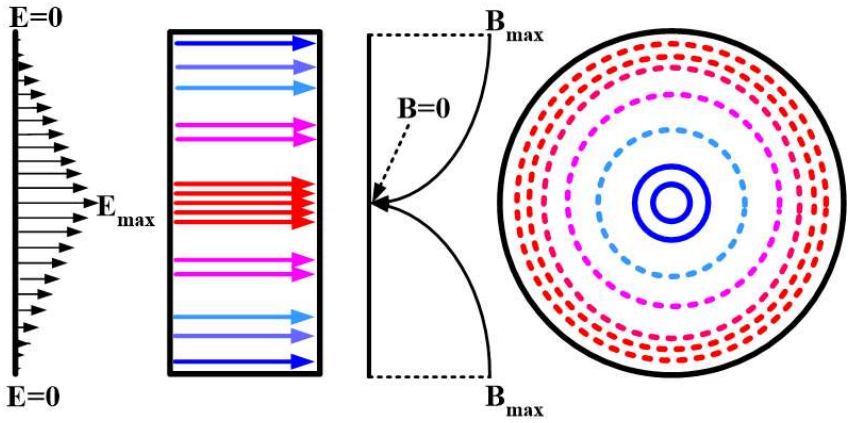

Figure 2.4: EM field distribution for the TM_{01} mode inside the cylindrical single-cell resonant structure [Miller (2006)].

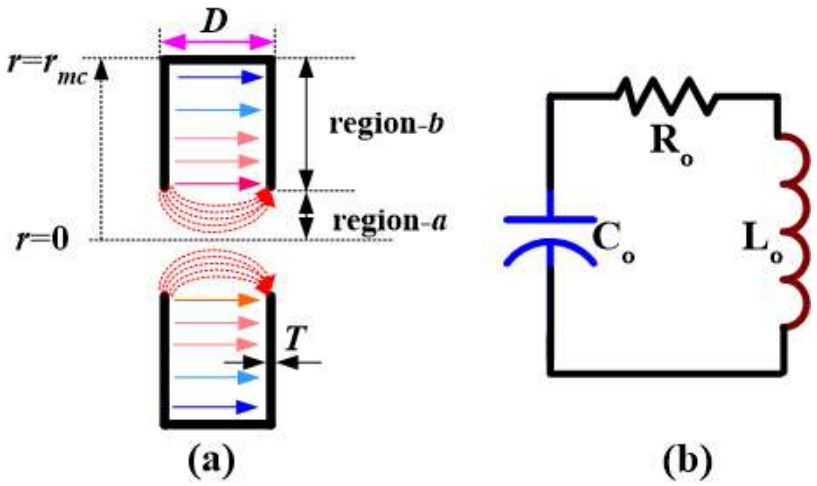

Figure 2.5: (a) Electric field distribution inside the single-cell resonant structure, and (b) its equivalent circuit.

The dominant mode of the SCC structure is TM_{01} mode and considered here for the analysis. For convenience, it is assumed that the electric field varied linearly in the TM_{01} mode. The magnitude of the electric field is higher at the center (i.e. at $r=0$) and decreases gradually with the increase in radius, and becomes zero at the cavity wall (i.e. at

$r = r_{mc}$). At the same time, the magnitude of the magnetic field in the TM_{01} mode is higher at the cavity's wall (i.e. at $r = r_{mc}$), and continuously decreases and becomes zero at the center of the cavity (i.e. at $r = 0$) [Miller (2006)].

The EM field distribution for the TM_{01} mode inside the cylindrical single-cell resonant structure is shown in Fig. 2.4. The equivalent circuit model for a single cell resonant structure is shown in Fig. 2.5 (b), and its fundamental resonating frequency for this equivalent circuit can be defined as:

$$\omega_{res} = \sqrt{\frac{1}{L_0 C_0}} \tag{2.1}$$

The adjacent main pillbox cavities are magnetically coupled through the radially connected coupled cavity and this magnetic coupling is represented by the transformer with the coupling factor (*k*). The coupling factor (*k*) is defined as:

$$k = \frac{M}{L_o} \quad \text{where} \quad 0 < k < 1 \tag{2.2}$$

where 'M' represents the mutual inductance. It is assumed that the current has an oscillatory solution $i = Ie^{j\omega t}$. Applying the Kirchhoff voltage law (KVL) in the leftmost circuit, we get [Miller (2006), Soh *et al.* (2010)]:

$$0 = R_o i_1 + L_o \frac{di_1}{dt} - kL_o \frac{di_1}{dt} - \frac{1}{C_o}\int i_1 dt \tag{2.3}$$

Solving the above equation and rearranging the above equation in terms of current, we get:

$$0 = R_o I_1 + j\omega L_o I_1 - j\omega k L_o I_2 - \frac{I_1}{j\omega C_o}$$

$$0 = I_1\left(R_o + j\omega L_o - \frac{I_1}{j\omega C_o}\right) - j\omega k L_o I_2$$

$$\left(\frac{\omega_{res}^2}{\omega^2} - 1 + \frac{jR_o}{\omega L_o}\right) I_1 + k I_2 = 0 \tag{2.4}$$

Similarly, applying the Kirchhoff voltage law (KVL) in the middle and rightmost circuit, and then by rearranging, we get:

$$\frac{k}{2}(I_1) + \left(\frac{\omega_{res}^2}{\omega^2} - 1 + \frac{jR_o}{2\omega L_o}\right) I_2 + \frac{k}{2}(I_3) = 0 \tag{2.5}$$

$$k I_2 + \left(\frac{\omega_{res}^2}{\omega^2} - 1 + \frac{jR_o}{\omega L_o}\right) I_3 = 0 \tag{2.6}$$

Equations (2.3)–(2.5) can be written in the matrix form [Miller (2006)]:

$$[A][I] = [0] \tag{2.7}$$

where '$[I]$' is a current vector, '$[0]$' is the zero vector, '$[A]$' is the matrix operator, and the elements inside the matrix are given as:

$$[A] = \begin{bmatrix} \left(\frac{\omega_{res}^2}{\omega^2} - 1 + \frac{jR_o}{\omega L_o}\right) & k & 0 \\ \frac{k}{2} & \left(\frac{\omega_{res}^2}{\omega^2} - 1 + \frac{jR_o}{2\omega L_o}\right) & \frac{k}{2} \\ 0 & k & \left(\frac{\omega_{res}^2}{\omega^2} - 1 + \frac{jR_o}{\omega L_o}\right) \end{bmatrix} \tag{2.8}$$

$$[I] = \begin{bmatrix} I_1 \\ I_2 \\ I_3 \end{bmatrix} \quad \textit{and} \quad [0] = \begin{bmatrix} 0 \\ 0 \\ 0 \end{bmatrix}$$

By putting the determinant of $[A]$ equal to zero and simplifying it, we have two sets of equations:

$$\left(\frac{\omega_{res}^2}{\omega^2}-1+\frac{jR_o}{\omega L_o}\right)=0 \tag{2.9}$$

$$\left[\left(\frac{\omega_{res}^2}{\omega^2}-1+\frac{jR_o}{\omega L_o}\right)\left(\frac{\omega_{res}^2}{\omega^2}-1+\frac{jR_o}{2\omega L_o}\right)-k^2\right]=0 \tag{2.10}$$

Since the ratio R_0/L_0 only serves to damp the oscillation field and with the assumption that the cell is loss-less (i.e. $R_0=0$) we can eliminate the effect of cavity resistance. Putting $R_0=0$ in expression (2.9), the first resonating frequency becomes equal to the fundamental resonating frequency of the single cell:

$$\omega_1=\omega_{res}=\omega_{\pi/2}=\sqrt{\frac{1}{L_oC_o}} \tag{2.11}$$

To obtain the current flow into the SCC we substitute the obtained ω_1 into expression (2.7):

$$i_1=I_1e^{j\omega_{res}t} \tag{2.12}$$

$$i_2=0 \tag{2.13}$$

$$i_3=-I_1e^{j\omega_{res}t} \tag{2.14}$$

From expression (2.12)–(2.14), it is observed that the current in the coupled cavity is zero, while the current in the adjacent main pillbox cavity is in the opposite direction which indicates that the electric field present in the adjacent main pillbox cavities have a phase shift of 180^o to each other. This type of electric field distribution in the SCC is obtained for π/2-mode [Knapp *et al.* (1965), Miller *et al.* (1995), Miller (2006)]. The other two

resonating frequencies have been obtained by putting $R_0 = 0$ and solving the expression (2.10), we get:

$$\omega_2 = \frac{\omega_{res}}{\sqrt{1+k}} \tag{2.15}$$

$$\omega_3 = \frac{\omega_{res}}{\sqrt{1-k}} \tag{2.16}$$

Theoretically, the magnetic coupling factor (k) can be obtained by rearranging the expression (2.15) and (2.16) expressed as [Miller (2006)]:

$$k = \left(\left(\frac{\omega_1}{\omega_2} \right)^2 - 1 \right), \quad \text{or} \tag{2.17}$$

$$k = \left(1 - \left(\frac{\omega_{res}}{\omega_m} \right)^2 \right) \tag{2.18}$$

2.3.1. Equivalent Inductance $\left(L_0\right)$

To calculate the equivalent inductance of the single cell of the system, it is assumed that the uniform current density (i.e. $J\left(r\right)$) exists in the hollow cylinder, and can be expressed as:

$$J(r) = J_0 \, \bar{a}_z \quad \text{for} \quad r_h \le r \le r_{mc} \tag{2.19}$$

According to Ampere's law, a cylindrically symmetric current density produces a magnetic flux density, and can be expressed as:

$$B(\bar{r}) = \frac{\mu_0 I_{enc}}{2\pi r} \hat{a}_\phi = \left(\frac{\mu_0}{r} \int_0^r J_z(r') \, r' \, dr' \right) \hat{a}_\phi \tag{2.20}$$

$$\int_0^r J_z(r')\,r'\,dr' = \int_0^{r_h} J_z(r')\,r'\,dr' + \int_{r_h}^r J_z(r')\,r'\,dr' \tag{2.21}$$

Therefore, the magnetic flux density in the hollow portion of the cylinder becomes

$$B(\bar{r}) = \frac{\mu_0 I_{enc}}{r} J_0\left(\frac{r^2 - r_h^2}{2}\right)\hat{a}_\phi \tag{2.22}$$

Assuming that the total current enclosed by the hollow cylinder is 'I_{enc}' which can be obtained by taking a surface integral of the current density '$J(r)$' across the cross-sectional surface 'S' of the hollow cylinder as:

$$I_{enc} = \int_0^{2\pi}\int_{r_h}^{r_{mc}} J_0\, r\, dr\, d\phi = J_0\pi\left(r_{mc}^2 - r_h^2\right) \tag{2.23}$$

Using expression (2.22) and (2.23), the final expression for the magnetic flux can be written as:

$$B(\bar{r}) = \frac{\mu_0 I_{enc}}{r} J_0\left(\frac{r^2 - r_h^2}{2}\right)\hat{a}_\phi \tag{2.24}$$

The total flux through the cross-section of the tube can be obtained by integrating magnetic flux density over the tube's radius, can be expressed as:

$$B(\bar{r}) = \frac{I_{enc}\mu_0}{4\pi\left(r_{mc}^2 - r_h^2\right)}\left(r_{mc}^2 - r_h^2 - 2r_h^2 \ln\left(\frac{r_{mc}}{r_h}\right)\right) \tag{2.25}$$

Since the inductance is defined as the ratio of the total magnetic flux to the current enclosed in the cross-section, the equivalent inductance of the hollow cylinder become:

$$L_o = \frac{\Phi}{I_{enc}} = \frac{\mu_0 D}{4\pi\left(r_{mc}^2 - r_h^2\right)}\left(\left(r_{mc}^2 - r_h^2\right) + 2r_h^2 \ln\left(\frac{r_h}{r_{mc}}\right)\right) \tag{2.26}$$

where 'μ_0', 'r_{mc}', and 'r_h' are free space permeability, the radius of the main pillbox cavity, and radius of disc hole, respectively.

2.3.2. Equivalent Capacitance (C_0)

The equivalent capacitance (C_0) of the single-cell system can be defined as the summation of the capacitances due to the disc-free and the disc-occupied regions [Fan *et al.* (1992)]. The electric field distribution in the single-cell resonant structure is shown in Fig. 2.5 (a). The capacitance in the disc-free region is calculated by assuming that the electric field lines are homocentric and semi-circular lines that exist at the center of the single-cell resonant structure. Between the two vanes in region-*a,* the potential difference (V_a) can be written as:

$$V_a = \frac{\pi r \sigma_{a,r}}{\varepsilon_0} \tag{2.27}$$

where '$\sigma_{a,r}$' is the charge per unit area in region-*a*. The surface charge in region-*a* becomes:

$$Q_{a,r} = \int_{H/2}^{H/2+W} \sigma_{a,r}(2\pi r_h)dr = 2\varepsilon_0 r_h V_a \ln\left(1+\frac{2T}{D}\right) \tag{2.28}$$

Hence, capacitance in region-*a* becomes:

$$C_a = \frac{Q_a}{V_a} = 2\varepsilon_0 r_h \ln\left(1+\frac{2T}{D}\right) \tag{2.29}$$

For the capacitance calculation due to the region-*b*, it is assumed that the electric field varies linearly along the radius of the single-cell resonant structure. The magnitude of the

electric field is higher at the center and starts decreasing as we move radially outward direction i.e. towards the wall of the cavity. Therefore, the electric field can be written as:

$$E_{\mathrm{b},r} = \frac{E_0(r_{mc} - r)}{(r_{mc} - r_h)} \tag{2.30}$$

The radial electric field, in accordance with Gauss's electrostatics law, in region-*b* (i.e. $E_{b,r}$) can be written as:

$$E_{b,r} = \frac{\sigma_{b,r}}{\varepsilon_0} \tag{2.31}$$

where, ε_0 (free space permittivity), $\sigma_{a,r}$ (the charge per unit area in region-*b*), and 'E_0' (magnitude of the electric field). The charge (Q_b) at the side surface is defined as:

$$Q_b = \int 2\pi r \sigma_{b,r} dr \tag{2.32}$$

$$Q_b = \frac{\pi\varepsilon_0 E_0}{3(r_{mc} - r_h)}\left(r_{mc}^3 + 2r_h^3 - 3r_{mc}r_h^2\right) \tag{2.33}$$

The average potential difference (V_b) across the two vanes:

$$V_b = \frac{E_0 D}{2} \tag{2.34}$$

where T, and D are the thickness and length and of the single-cell resonant structure cavity (Fig. 2.5). Hence, the capacitance in region-*b* becomes:

$$C_b = \frac{Q_b}{V_b} = \frac{\pi\varepsilon_0 E_0}{3(r_{mc} - r_h)D}\left(r_{mc}^3 + 2r_h^3 - 3r_{mc}r_h^2\right) \tag{2.35}$$

The equivalent capacitance (C_0) will be the sum of the capacitances in the region-*a*, and region-*b*:

$$C_0 = \left(C_a + C_b\right) = \left(2\varepsilon_0 r_h \ln\left(1+\frac{2T}{D}\right)\right) + \left(\frac{\pi\varepsilon_0 E_0}{3\left(r_{mc}-r_h\right)D}\left(r_{mc}^3 + 2r_h^3 - 3r_{mc}r_h^2\right)\right) \qquad (2.36)$$

2.3.3. Expression for the Magnetic Coupling Coefficient

The equivalent circuit model of the SCC is presented in Fig. 2.2, where '*k*' represents the magnetic coupling factor between the adjacent main pillbox cavities [Knapp *et al.* (1965)]. From Fig. 2.1**,** it can be observed that the area associated with the magnetic coupling slot mainly depends upon the coupling depth. Therefore, for any variation in the coupling-depth changes the corresponding angle value (i.e. the value of 'ψ' and 'ϕ'), as a result, the amount of magnetic coupling present in the SCC also varies. According to the perturbation theory, any addition or subtraction in the cavity's area changes the RF current flow in the cavity [Carter *et al.* (1986), Carter (2018)]. This RF current variation changes the cavity inductance, and as a result; there is a change in the SCC's resonating frequency.

Let us assume that the total RF current $\left(I_0\right)$ flows in the main cavity of the SCC when there was no perturbation. The overlapped area between the coupling-cavity and the main pillbox cavity and that of the SCC mainly depends upon the coupling depth. This overlapped area gets removed to form a magnetic coupling slot. The relation between the coupling depth and the magnetic coupling slot area is visualized with the help of Fig. 2.1. The removed overlapped area that depends primarily on the coupling depth from the periphery of the main pillbox cavity is used to provide the magnetic coupling through the coupling cavity between the adjacent main pillbox cavities. According to the perturbation theory, some fraction of the total RF circulating current is involved in the coupling. This fraction of the RF current is responsible for magnetic coupling and is called a magnetic coupling factor (*k*). This coupling factor can be described as the ratio of the total removed

area for making a slot from the main pillbox cavity to the total unperturbed area [Carter *et al.* (1986), Carter (2018)];

$$k = \frac{\left(\text{Removed Area for Making slot}\right)}{\text{Total Unpertubated Area of the Main Cavity}} \tag{2.37}$$

The detailed analysis to obtain the magnetic coupling factor is given in Appendix-A. The final expression for the magnetic coupling factor (k) in terms of SCC's structural parameter is:

$$k = \frac{\left(360\, r_{mc}\, D\phi\right)}{\pi\left(\left(2\, r_{mc}\, D\right)+\left(r_h\, T\right)+\left(r_{mc}^2 - r_{cc}^2\right)\right)} \tag{2.38}$$

2.3.4. Simulation Study of Coupling Depth

The S-band SCC structure is modeled according to the structural dimension mentioned in Table 2.1 with the help of "CST Studio Suite". The scattering parameter behavior of the structure is investigated by simulating the SCC structure in the frequency-domain solver. The input/output port is defined by selecting the edge of the coaxial probe as shown in Fig. 2.1 (b). The convergence criterion for the scattering coefficient is defined by choosing the accuracy ~10^{-6} (i.e. -60 dB) in the simulation, as soon as the scattering parameters arrive at about −60 dB, the numerical simulation will complete, converge and give the value of the scattering parameters. The S_{11} parameter obtained from the frequency-domain solver at different coupling depths is shown in Fig. 2.6. From the figure, it is evident that there are three dips and each dip is accompanying by the different resonating modes of the SCC. The marker is only attached with the π/2-mode (i.e. fundamental resonating mode frequency) to visualize the effect of coupling depth.

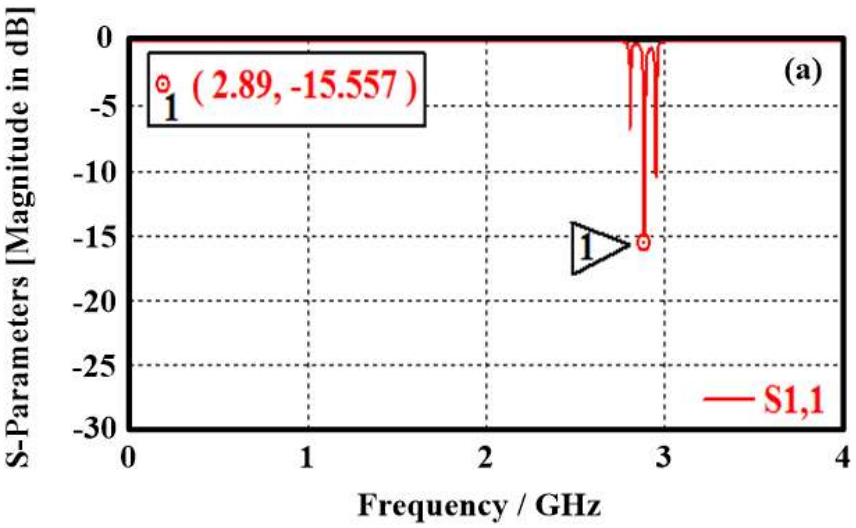
S-Parameters [Magnitude in dB]
0
-5
-10
-15
-20
-25
-30
0
1
2
3
4
Frequency / GHz
1 (2.89, -15.557)
(a)
1
S1,1

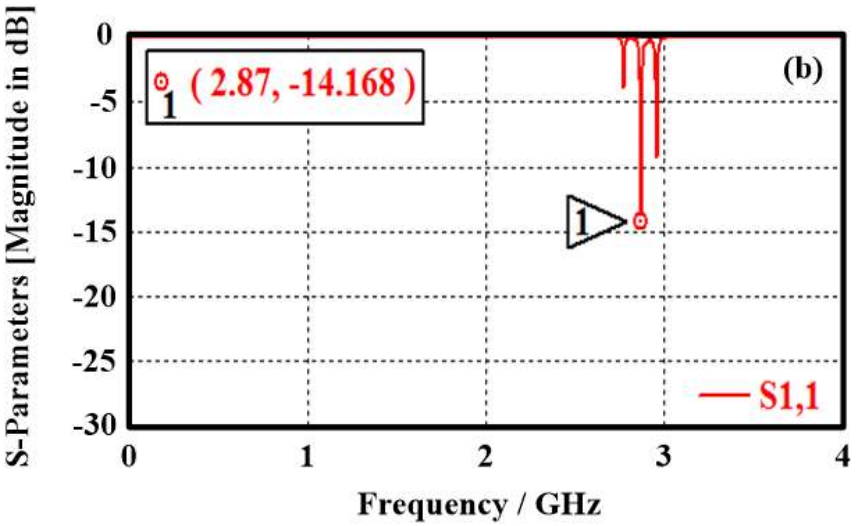
S-Parameters [Magnitude in dB]
0
-5
-10
-15
-20
-25
-30
0
1
2
3
4
Frequency / GHz
1 (2.87, -14.168)
(b)
1
S1,1

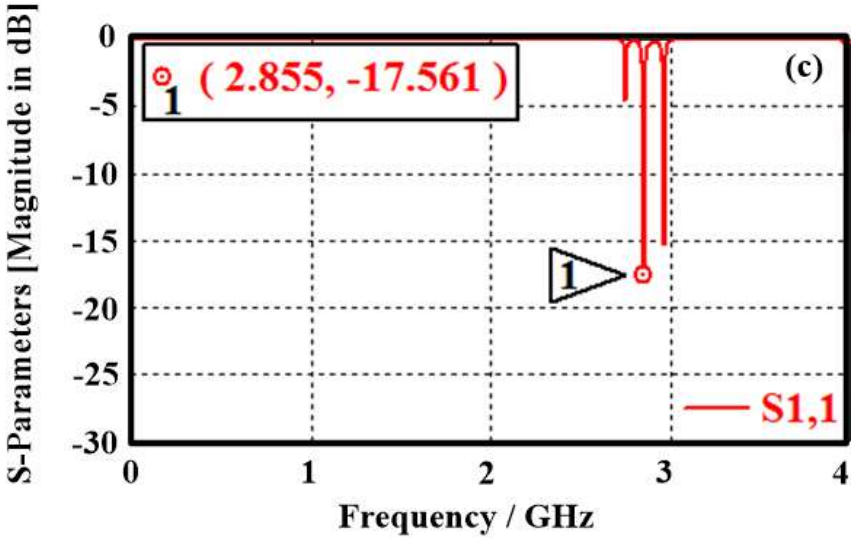
S-Parameters [Magnitude in dB]
0
-5
-10
-15
-20
-25
-30
0
1
2
3
4
Frequency / GHz
1 (2.855, -17.561)
(c)
1
S1,1

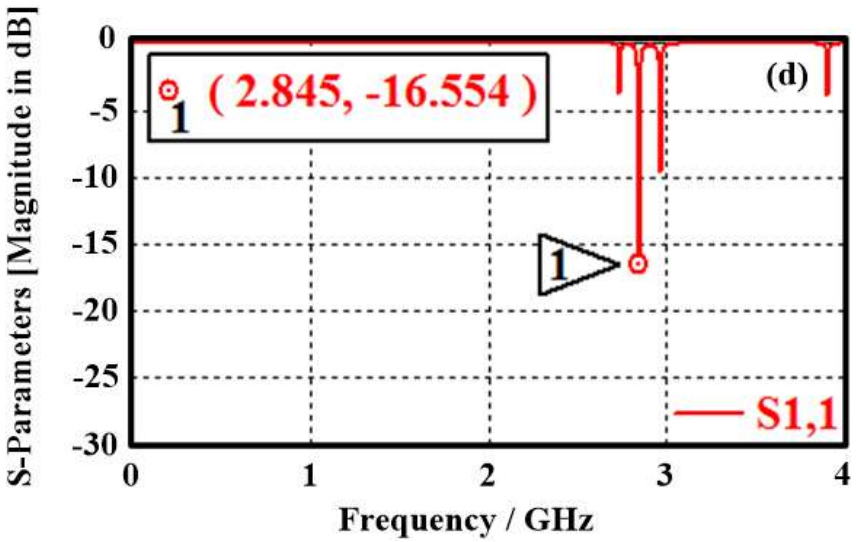

Figure 2.6: S_{11} parameter of the modeled SCC structure at different coupling depths: (a) at 6.0 mm, (b) at 7.6 mm, (c) at 8.6 mm, and (d) at 9.2 mm.

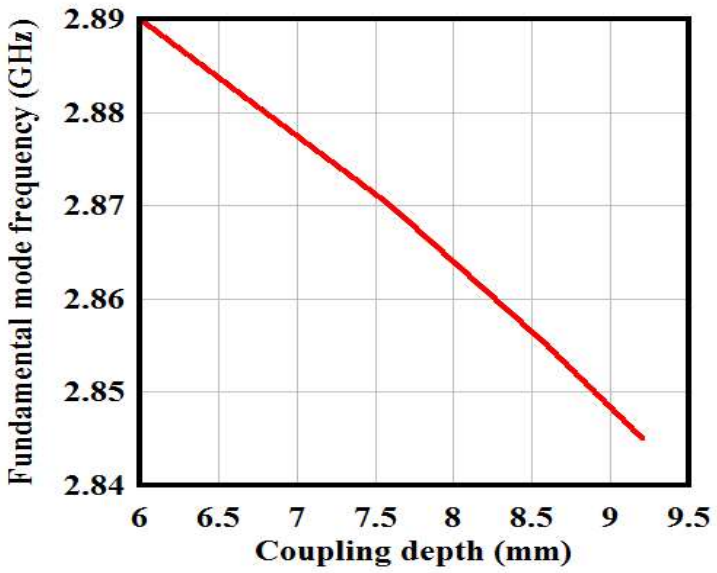

Figure 2.7: Effect of coupling depth on the resonating frequency associated with the π/2-mode.

The effect of coupling depth on the fundamental mode frequency (i.e. π/2-mode) is also shown in Fig. 2.7. From the figure, it gathered that with the increase in coupling depth,

the resonating frequency of the fundamental resonance mode (i.e. ω_1) decreases. The effect of coupling depth is also verified after analyzing Fig. 2.6 (a)–(d). Finally, from the simulation study, we conclude that any change in the coupling depth changes the coupling factor (k), which consequently changes the resonating frequency associated with the fundamental resonance mode. Roy *et al.* also observed the exact phenomenon in their experimental analysis [Roy *et. al.* (1993)].

2.3.5. Empirical Expression for π/2-mode

From the expression (2.11), it is observed that the fundamental resonating mode frequency (i.e. $\omega_1 = \omega_{res}$) depends only upon the value of equivalent capacitance and equivalent inductance. From the expression of equivalent inductance and equivalent capacitance (i.e. expression (2.26) and (2.36), respectively) it is seen that the expression does not include any terms of the magnetic coupling factor (k). Therefore, the frequency of the fundamental mode is independent of the magnetic coupling depth (i.e. magnetic coupling factor (k)). But simulation and experimentally reported studies suggested that the coupling depth alters the frequency associated with the fundamental resonance mode [Roy *et al*. (1993)]. To resolve this flaw, it is essential to include the effect of the magnetic coupling factor (k) in the expression (2.11). Therefore, an empirical expression is proposed to calculate the frequency associated with the fundamental resonance mode, which includes the effect of the magnetic coupling factor (k):

$$\omega_1 = \omega_{res} = \omega_{\pi/2} = \frac{1}{\sqrt{L_o C_o}}\left(f\left(k\right)\right) \tag{2.39}$$

where '$f\left(k\right)$' is an empirical expression that depends on the magnetic coupling factor.

$$f(k) = \left(1 - (2k) - (2k)^2 - (2k)^3 - (2k)^4 - .....\right) \quad (2.40)$$

Table 2.2: Comparison of simulated and numerically obtained results at different coupling depths.

Coupling Depth (in mm)	Resonating frequency of the π/2-mode using equation (1) (in GHz)	Resonating frequency of the π/2-mode obtained from EM simulation (in GHz)	Resonating frequency of the π/2-mode obtained using the proposed empirical formula (39) (in GHz)	Magnetic coupling factor (*k*) obtained using the proposed expression (38)	The relative error between the simulation and proposed empirical expression results (in %)
6.0	3.075	2.890	2.898	0.027	0.270
7.6	3.075	2.870	2.875	0.031	0.170
8.6	3.075	2.855	2.862	0.032	0.240
9.2	3.075	2.845	2.855	0.034	0.350

2.4. Validation of Theoretical Analysis

Results obtained through various techniques i.e. results obtained through simulation, results obtained from the expressions reported in Miller (2006), and results obtained from the proposed empirical expressions are comparatively listed in Table 2.2. From Table 2.2, the simulation and experimentally reported studies proved that increasing the coupling depth increases the value of the magnetic coupling factor (Because any change in coupling depth changes the associated value of 'ψ' and 'ϕ', as a result, the area associated with the

magnetic coupling slot also changes). The fundamental resonating mode frequency, calculated from the reported expression remains constant as the change in the coupling depth. To resolve this flaw, an empirical expression for the fundamental resonating mode frequency has been proposed (i.e. expression (2.39)).

To check the accuracy of the proposed empirical expression the results have been compared with the simulation results and from this comparison, it is observed that the relative error is less than 1%, which validates the accuracy of the proposed empirical expression.

2.5. Conclusion

In this chapter, the fundamental resonating mode frequency i.e. the frequency associated with the $\pi/2$-mode of the pillbox cavity-based SCC has investigated theoretically using an equivalent circuit approach. An expression is developed to calculate the magnetic coupling factor (k) in terms of their structural parameters. This theoretical analysis provides an alternative approach to calculate the value of the magnetic coupling factor, thereby providing a reference value of its design and for experimental verification. Furthermore, an empirical expression has also been proposed to estimate the resonating frequency associated with the fundamental mode, in which the effect of the magnetic coupling factor is included. The proposed empirical expression to calculate the resonating frequency associated with fundamental mode removes the flaws, which exist in the previously reported expression. The results obtained from the proposed empirical expression and simulation were compared to validate the derived theoretical analysis. The relative error between the simulated and the proposed empirical expression was 1%, which shows good agreement and validates the performed theoretical analysis.